2018

Slowdown of surface diffusion during early stages of bacterial colonization

T. Vourc'h

H. Peerhossaini

J. Leopoldes

A. Mejean

F. Chauvat

See next page for additional authors

Slowdown of surface diffusion during early stages of bacterial colonization

T. Vourc'h and H. Peerhossaini*
Laboratoire AstroParticules et Cosmologie, CNRS, Université Paris–Diderot, Université Sorbonne Paris Cité, 5 Rue Thomas Mann, 75013 Paris, France

J. Léopoldès†
ESPCI Paris, PSL Research University, CNRS, Institut Langevin, 1 Rue Jussieu, 75005 Paris, France and Université Paris–Est Marne-la-Vallée, 5 Boulevard Descartes, Champs sur Marne, Marne-la-Vallée Cedex 2, France

A. Méjean
Laboratoire Interdisciplinaire des Énergies de Demain, CNRS, Université Paris–Diderot, Université Sorbonne Paris Cité, 5 Rue Thomas Mann, 75013 Paris, France

F. Chauvat and C. Cassier-Chauvat
Laboratory of Biology and Biotechnology of Cyanobacteria. Institute for Integrative Biology of the Cell, CEA, CNRS, Université Paris–Sud, Université Paris–Saclay, 91198, Gif-sur-Yvette Cedex, France

(Received 10 November 2017; published 14 March 2018)

We study the surface diffusion of the model cyanobacterium *Synechocystis* sp. PCC6803 during the incipient stages of cell contact with a glass surface in the dilute regime. We observe a twitching motility with alternating immobile tumble and mobile run periods, resulting in a normal diffusion described by a continuous-time random walk with a coefficient of diffusion D. Surprisingly, D is found to decrease with time down to a plateau. This is observed only when the cyanobacterial cells are able to produce released extracellular polysaccharides, as shown by a comparative study between the wild-type strain and various polysaccharides-depleted mutants. The analysis of the trajectories taken by the bacterial cells shows that the temporal characteristics of their intermittent motion depend on the instantaneous fraction of visited sites during diffusion. This describes quantitatively the time dependence of D, related to the progressive surface coverage by the polysaccharides. The observed slowdown of the surface diffusion may constitute a basic precursor mechanism for microcolony formation and provides clues for controlling biofilm formation.

DOI: 10.1103/PhysRevE.97.032407

I. INTRODUCTION

In nature, bacteria develop preferentially in contact with solid surfaces by forming biofilms, i.e., masses of adherent cells embedded in slimy extracellular matrices. Biofilms are essential to bacterial growth and survival to environmental stresses. They capture nutrients in the vicinity of the cells and the peripheral cells exposed to the noxious agents protect the internal cells [1,2]. Biofilms also develop in many industrial and medical situations and their formation is a key mechanism in the infection of a living host by pathogenic organisms [3–5].

The biofilm structure depends critically on mass transport, surface chemistry, and surface topology [6]. The initial contact of the bacteria with the surface is followed by the formation of microcolonies [7]. Then the three-dimensional morphology of the mature film develops and chemical signaling triggers the release of bacteria in the liquid medium, which are then transported to other colonization sites via the flow of the liquid medium [8].

Bacteria are known to produce high-molecular-weight polymeric substances such as extracellular polysaccharides (EPSs) [9], which play important roles during the main stages of biofilm formation. For example, the mature biofilm contains the macromolecules adsorbed on the solid substrate which provide mechanical stability and adhesion. A distinction can be made between capsular EPSs (firmly bound to the outer cell membrane) and released EPSs (easily detached from the outer cell membrane) [10]. Moreover, it has been proved recently that the polysaccharides excreted by motile bacteria form attracting trails, giving rise to spatial accumulation of the cells, thereby yielding the localized growth of microcolonies [11–13]. The production of EPSs is also linked to the emergence of peculiar dynamics during the initial stages of surface colonization by altering the distribution of the velocity of bacterial cells [14].

In this work we study the relationship between excreted EPSs and the diffusion coefficient D at the early stages of surface colonization. Investigations are carried out with the unicellular cyanobacterium *Synechocystis* sp. PCC6803, a model of environmentally important photosynthetic prokaryote that produces EPSs in various forms [10,15]. The motility of *Synechocystis* on solids relies on the action of type IV pili [11,16–19] (the pili extend, bind on the solid surface, and then

*hassan.peerhossaini@univ-paris-diderot.fr
†julien.leopoldes@espci.fr

retract). Results collected for the wild-type cells are compared with those obtained with different mutant strains described elsewhere [10].

Surface motion occurs by the usual twitching motility but the diffusion coefficient is observed to decrease systematically with time down to a plateau. This effect is observed only with the wild-type and the Δ*sll1581* mutant strain, both able to produce released exopolysaccharides. This is not noticed for two double-mutant strains (Δ*sll581-sll1875* and Δ*sll0923-sll5052*) that produce a lower amount of released EPSs. We propose an interpretation that takes into account the coverage of the solid surface by the trails of the excreted EPSs. This affects the temporal characteristics of the intermittent twitching motility of the cells. We believe that such a process constitutes an important step in the adaptation of microorganisms to hard surfaces prior to the formation of microcolonies and biofilms.

II. MATERIALS AND METHODS

A. Bacterial suspensions and measurement of cell motion

The wild-type (WT) strain of the model cyanobacterium *Synechocystis* sp. PCC6803 was obtained from the Pasteur Institute, while the EPS-depleted single mutant (Δ*sll1581*) and double mutants (Δ*sll581-sll1875* and Δ*sll0923-sll5052*) were previously constructed by Jittawuttipoka *et al.* [10]. The three mutant strains produce less capsular EPSs than the WT cells. The amount of released EPSs produced by the single mutant (Δ*sll1581*) is similar to that of the WT cells; both double mutants (Δ*sll1581-sll1875*) and (Δ*sll0923-sll5052*) form less released EPSs.

All strains are routinely cultured in the BG11 standard mineral medium and subcultivated by diluting 3 mL of a mother culture in 47 mL of fresh BG11. The suspensions are stirred by a magnetic agitator operating at 360 rotations per minute in a clean room at 20 °C. They are placed under white light of an intensity of 1.3 W m^{-2} for 7 days followed by 24 h of darkness and a subsequent 2 h of light before running the experiments. At this stage, the concentration of cyanobacteria is approximately 2×10^7 cells per mL. The suspensions are diluted from twofold to tenfold in fresh BG11 before introduction in the measurement chamber. With this protocol, some of the cells are dividing, which results in an average particle diameter $d \sim 3$ μm, slightly larger that single cells, whose size is approximately 2 μm.

Experiments are conducted in two different systems as represented in Fig. 1. One measurement cell consists in a BRAND® cavity microscope slide (26×76 mm^2) closed by a coverslip (Menzel-Gläser, 22×22 mm^2) and sealed with high-vacuum grease [Fig. 1(a)]. The second measurement cell is a Y-junction microfluidic channel of cross section 100×205 μm^2 [see the protocol detailed in Fig. 1(b)].

B. Cell tracking

The cyanobacterial cells are observed with a homemade inverted microscope equipped with a Nikon TU Plan 10× objective and a white light source. Their motion is recorded with a monochrome camera (Edmund Optics) at one frame per second. The recordings are postprocessed with IMAGEJ software to obtain binary images and then analyzed for particle tracking [20] with MATLAB. Only trajectories whose duration is longer than 250 s are retained for further analysis, while the few nonmotile cells are ignored. The number of analyzed trajectories is 9843 in Sec. III A, 453 in Sec. III B, and 1424 for the experiments in the microfluidic chip. Details on the computation of the mean-square displacement (MSD) are given in Appendix A.

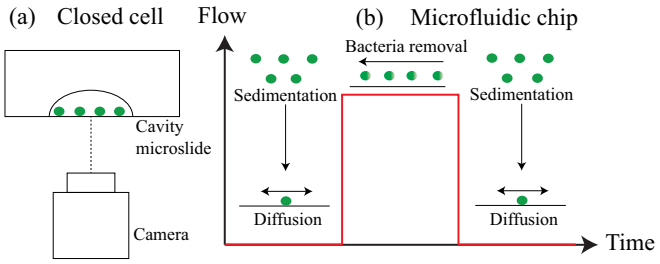

FIG. 1. Experimental setup. (a) Closed cavity where the bacterial cells (dots) sediment and diffuse on the lower surface. (b) Protocol followed with the microfluidic cell: The first experiment is carried out similar to that in (a) but in a microfluidic cell with controllable flow. After sedimentation is completed and having let the bacteria diffuse enough on the lower surface, a pressure gradient is applied to detach the cells from the surface. Then the flow is stopped and the sedimentation-diffusion process starts again. In both setups, bacterial cells are observed with the same equipment (optical microscope coupled to a CCD camera).

III. RESULTS

A. Cell transport, contact with a solid surface, and slowdown of motion

Data recording starts a short time after the introduction of the cyanobacterial cells in the measurement chamber. Due to cell sedimentation, the number $N(t)$ of bacterial cells detected on the hard surface increases with observation time t until a final value N_∞ is reached [see Fig. 2(a)]. The sedimentation process is reproducible and can be described by the empirical law

$$N(t) = N_0 + (N_\infty - N_0)(1 - e^{-t/\tau_N}), \qquad (1)$$

where $\tau_N = 2081 \pm 4$ s and N_0 is the initial number of bacteria at the surface. The characteristic time for sedimentation τ_N can be obtained from the Stokes velocity $v_S = \Delta\rho g V_p / 6\pi\eta R$, where $\Delta\rho$ is the density contrast between the bacterial cells and the culture medium, g is the acceleration of gravity, V_p is the volume of the bacterial cells, R is their radius, and $\eta \approx 10^{-3}$ Pa s is the dynamical viscosity of the suspension as measured by means of a horizontal capillary. With $\Delta\rho = 100$ kg m^{-3} [21], $g = 9.81$ m s^{-2}, $R = 1.5$ μm, and the height of the cell $h = 1$ mm, we obtain $\tau_N \sim 2000$ s, consistent with experiments.

The dynamics of surface motion is first described by computing the mean-square displacement during a short-time interval $10 < \Delta < 80$ s, as a function of the observation time t [Eq. (A1)]. Figure 2(b) indicates that this short-time MSD is a linear function of Δ for all observation times t, as for Fickian diffusion. However, the corresponding

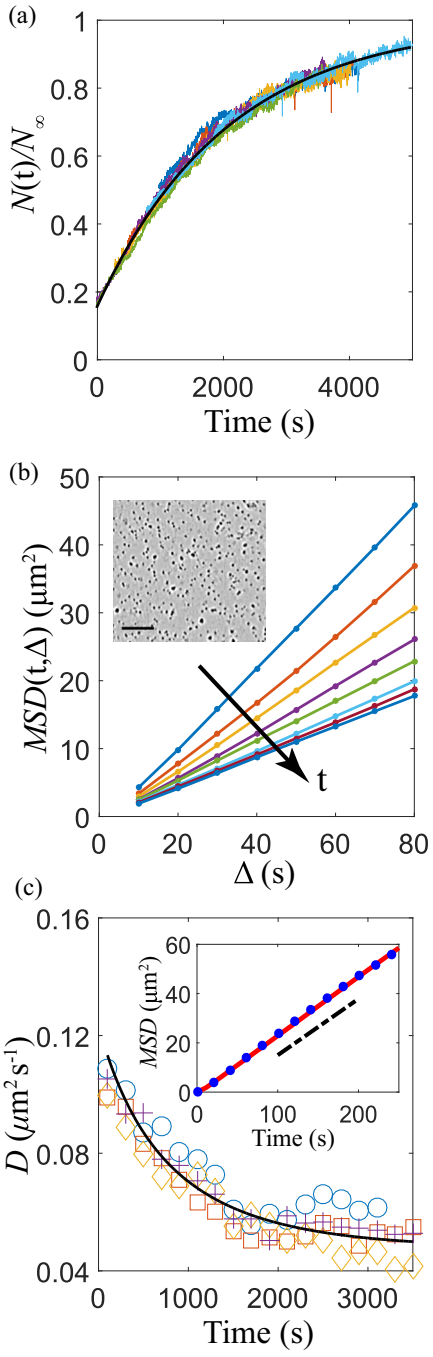

FIG. 2. (a) For five different experiments, temporal evolution of the number of cyanobacterial cells detected on the hard surface divided by the final number of cells. The plain line corresponds to Eq. (1). (b) Mean-square displacement at several observation times for a selected experiment, computed according to Eq. (A1). The MSD is plotted for observation times ranging from $t = 100$ to 2900 s in steps of 400 s. Increasing observation time is indicated by the arrow. The inset shows a snapshot of a typical experiment where bacteria appear as dark spots on the gray background (scale bar 50 μm). (c) Symbols show the temporal evolution of the diffusion coefficient for experiments similar to (a); the black line is the fit based on Eqs. (2) and (3) (see the discussion Sec. IV C for details on the fitting procedure). The inset shows the experimental MSD at long times (circles) and as computed from numerical simulations (line). The dashed black line indicates the slope given by Eq. (2).

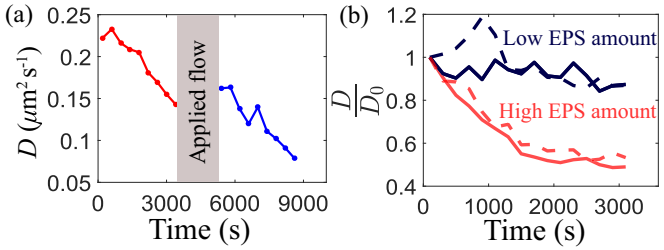

FIG. 3. (a) Temporal evolution of the coefficient of diffusion for experiments carried out in the microfluidic system [see Fig. 1(b)]. Renewal of the bacterial cell population due to the liquid flow occurs during the period corresponding to the vertical gray bar. (b) Temporal evolution of the diffusion coefficient normalized by its initial value D_0 for various *Synechocystis* strains. Data are the result of averaging over two different experiments. The black (dark) dashed line shows Δ*sll*1875-sll1581, the black (dark) solid line Δsll0923-sll5052, the red (light) solid line the wild type, and the red (light) dashed line Δsll1581.

time-dependent diffusion coefficient $D(t)$ defined by $\mathrm{MSD}(t,\Delta) = 4D(t)\Delta$ decreases with t. Such a slowdown of the dynamics, which constitutes the main result of this work, is reported in Fig. 2(c) for different experiments, showing a systematic gradual decrease of $D(t)$ until a plateau is reached at $D_\infty \approx 0.053 \pm 0.006\ \mu\mathrm{m}^2\ \mathrm{s}^{-1}$ after approximately 2500 s. Here D_∞ is independent of the instantaneous bacterial surface density in the range explored here (10^9–10^{10} particles/m^2). This corresponds to a surface fraction less than 8% and a typical interparticle distance of at least 10 μm, larger than the average cell diameter $d \sim 3\ \mu$m [see Fig. 2(b), inset].

Figure 3(a) shows the results obtained with the microfluidic system, which is used to renew the population of bacteria in the surface vicinity without changing the surface on which diffusion occurs. After the introduction to the microfluidic cell, the cyanobacteria are allowed to sediment and diffuse onto the surface without applied flow. The observed trend is similar to the experiments in the closed chamber: The diffusion coefficient decreases with time. After about 1 h of surface diffusion, the cells are detached from the surface by establishing a fluid flow for 20 min [vertical gray bar in Fig. 3(a)]. Then the flow is stopped and the cells are allowed to sediment and diffuse onto the surface again. The diffusion coefficient takes the same value as what was found just before the washing flow. Since the population of cells was totally renewed by the washing flow, this observation suggests that the surface has retained a signature of the past diffusion events, which influences the behavior of the new incoming cells.

Moreover, we find that the time evolution of the diffusion coefficient is highly dependent on the ability of *Synechocystis* to produce released EPSs [see Fig. 3(b)]. The wild-type and the single mutant Δ*sll1581* strains, which produce similar high quantities of released EPSs as compared to the two double-mutant strains (Δ*sll1581-sll1875* and Δ*sll0923-sll5052*), are characterized by the significant decrease of about 60% of the initial diffusion coefficient. In contrast, the Δ*sll1581-sll1875* and Δ*sll0923-sll5052* double mutants, which produce much less released EPSs, exhibit a smaller decrease of 10% in their

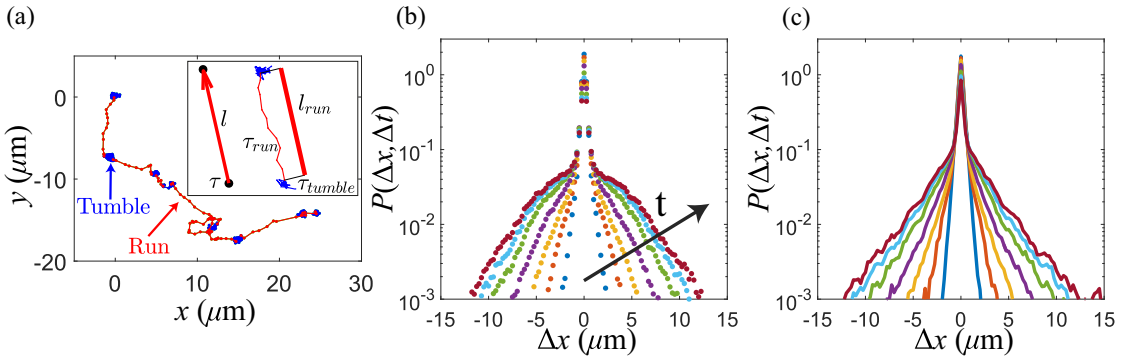

FIG. 4. (a) Trajectory of a bacterial cell (668 s). Runs correspond to (red) lines and tumble to (blue) dots. The inset shows a representation of a diffusion step by the continuous-time random-walk model (left) and the corresponding experimental diffusion step where the distance traveled during a run l_{run}, the corresponding run duration τ_{run}, and the tumble duration τ_{tumble} are indicated (right). Also shown are displacement probabilities along one direction for (b) experimental trajectories at the plateau and (c) simulated trajectories. The distributions are given for time intervals $\Delta = 2, 5, 10, 20, 40, 60$, and 80 s. Increasing time interval is indicated by the arrow.

diffusion coefficient. Hence, the released EPSs are identified as a major cause for the slowdown of the cell dynamics.

B. Normal diffusion resulting from twitching motility

We now focus on the permanent regime once the plateau has been reached and analyze the trajectories of the bacterial cells for a representative experiment which will be referred to as experiment 1. Figure 2(c) (inset) displays the linearity of the mean-square displacement (A2) for the representative experiment with a diffusion coefficient at the plateau $D_{\infty,1} = 0.059 \pm 0.001\ \mu\text{m}^2\,\text{s}^{-1}$. Yet the apparently normal surface diffusion of *Synechocystis* stems from the complex dynamics illustrated by the non-Gaussian probability distribution function (PDF) of displacement shown in Fig. 4(b). The central part of the distribution corresponds to a state of low mobility (tumble), while the tails reflect the higher cell mobility occurring during the run periods [22,23]. A typical trajectory in Fig. 4(a) indeed reveals twitching motility with run and tumble motion. The run periods are directional and detected with the procedure explained in Appendix B, from which we obtain the run times τ_{run} and additionally the tumble times τ_{tumble} and the mean velocity of runs, defined as $V_m = l_{\text{run}}/\tau_{\text{run}}$, where l_{run} is the distance traveled during the run.

We conduct numerical simulations in order to check for the relevance of the detection procedure (see details in Appendix C). First, we fit the experimental distributions of run and tumble time as in Fig. 9 (Appendix C). Additionally, we assume that runs are *ballistic* excursions of length $l_{\text{run}} = \tau_{\text{run}} \times V_m$, as suggested by experiments. Then, for each step of the simulation, τ_{run}, τ_{tumble}, and V_m are chosen randomly along the fits of the experimental distributions. This reproduces the experimental displacement PDF, as shown by comparing Figs. 4(b) and 4(c), and provides a diffusion coefficient from simulations $D_{\text{simu}} \approx D_{\infty,1}$ [inset of Fig. 2(c)].

Details on the slowdown of motion are provided by analyzing the time variation of $\langle\tau_{\text{run}}\rangle$, $\langle\tau_{\text{tumble}}\rangle$, and $\langle V_m\rangle$ (here angular brackets indicate a time average over temporal windows of 200 s), plotted Figs. 5(a), 5(b), and 5(c), respectively. For the wild-type and the $\Delta sll1581$ mutant that produce released EPSs, $\langle\tau_{\text{run}}\rangle$ decreases and $\langle\tau_{\text{tumble}}\rangle$ increases with time. This is not observed with the two double mutants that produce less released EPSs and their tumble and run times are almost constant. Importantly, $\langle V_m\rangle$ is not only similar but also constant for all the bacterial strains studied.

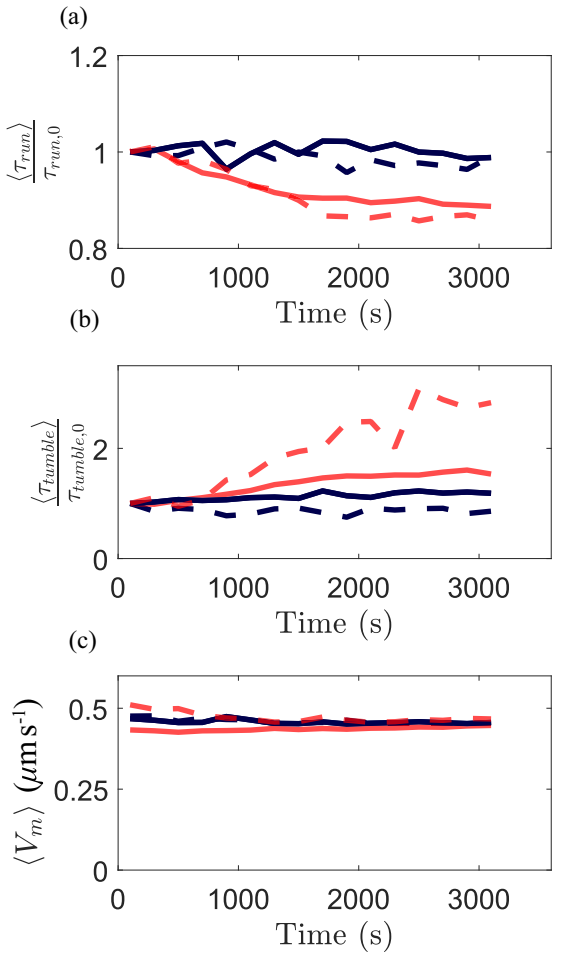

FIG. 5. Temporal evolution of (a) $\langle\tau_{\text{run}}\rangle$, (b) $\langle\tau_{\text{tumble}}\rangle$, and (c) $\langle V_m\rangle$. Here $\overline{V}_m$ is indicated by the arrow. Data are normalized by their initial value for the various *Synechocystis* strains. The lines are defined as in Fig. 3(b).

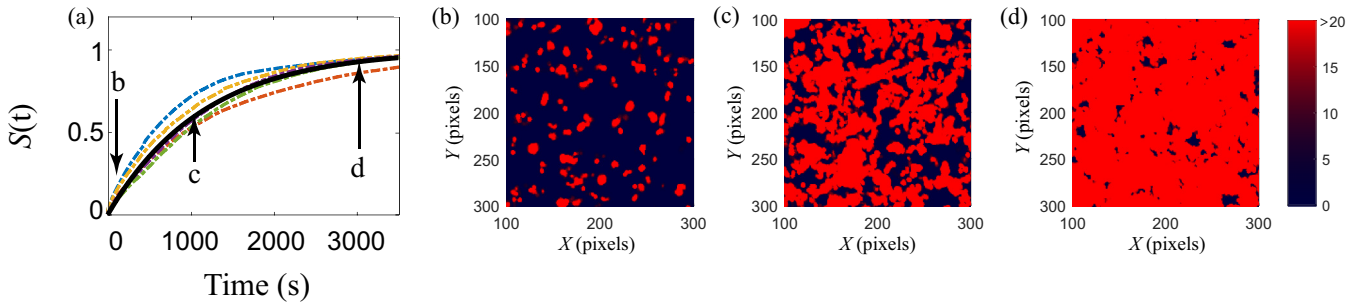

FIG. 6. (a) Fraction of surface area covered by trajectories in various experiments as a function of time (dot-dashed lines). The thick black solid line is a curve fitted with Eq. (3) (see the discussion in the text). (b)–(d) Colonization maps of the surface for the times indicated in (a). Colormaps indicate the cumulated number of visits in the considered pixel (dark areas indicate empty sites whereas bright areas indicate sites visited more than 20 times).

C. Surface area covered by trajectories

As a basic step for early stages of biofilm formation, we analyze how the surface is explored by the diffusing bacteria. The images are binarized such that the bacteria appear as black disks on a white background and every black pixel is given a value of 1 (zero otherwise). The cumulated number of visits for each pixel at a given time is then obtained by summing iteratively all preceding images. Figures 6(b)–6(d) display how the surface area is progressively filled by the trajectories of the diffusing bacteria during the time scale of the experiment. Moreover, although the experiments are conducted in the dilute regime, the fraction of distinct sites (pixels) visited $S(t)$ tends to 1, meaning that the whole surface area of the sample can be screened by EPSs. Figure 6(a) points out the robustness of this feature.

IV. DISCUSSION

A. Dynamics

The fact that the average velocity of runs $\langle V_m \rangle$ is common to all cyanobacterial strains used in this study implies that it is not linked to the production of EPSs and calls for a simple estimate based on lubrication theory. The motion of cyanobacterial cells is ensured by the traction of type IV pili which provides the force F necessary to shear a layer of fluid of viscosity η and thickness h squeezed between the bacteria and the surface, leading to $F \sim a\eta V/h$, where $a \sim \pi R^2$ is the sheared area ($R = 1.5\,\mu$m is the radius of a bacterial cell). With $V \sim 1\ \mu\text{m s}^{-1}$ the maximum velocity during runs, $h \sim 1$ nm the thickness of the sheared layer, and $\eta \sim 1 \times 10^{-3}$ Pa s the dynamical viscosity, we obtain the force exerted by the pili $F \sim 7$ pN, consistent with the order of magnitude obtained from mechanical testing with atomic force microscopy [24]. The velocity of the bacterial cells during run periods is thus limited by the viscous dissipation of the sheared water (liquid mineral medium BG11) layer at the interface between the bacterial cells and the solid surface.

B. Continuous-time random walk

The diffusion coefficient at long times may be obtained by considering a continuous-time random walk, where the particle jumps instantaneously over a length l after a waiting time τ [25,26], as illustrated in the inset of Fig. 4(a). We have computed both $l = l_{\text{run}}$ and $\tau = \tau_{\text{run}} + \tau_{\text{tumble}}$ (taken consecutively) and verified that the second moment of the jump length PDF and the first moment of the waiting-time PDF exist. Then the diffusion coefficient takes the simple expression $D = \langle l^2 \rangle / 4\langle \tau \rangle$. Ballistic runs occurring at constant velocity $\overline{V}_m \sim 0.47 \pm 0.3\ \mu\text{m s}^{-1}$ [see Fig. 5(c)] suggest the approximation $\langle l^2 \rangle \approx \overline{V}_m^2 \langle \tau_{\text{run}}^2 \rangle$. Therefore, an expression for the diffusion coefficient reads

$$D \sim \frac{1}{4}\overline{V}_m^2 \frac{\langle \tau_{\text{run}}^2 \rangle}{\langle \tau \rangle}. \tag{2}$$

The computation of the PDF for $\tau_{\infty,1}$ and $\tau_{\text{run},\infty,1}^2$ leads to well-defined average quantities but without a second moment. To calculate D from Eq. (2) we use therefore $\langle \tau_{\infty,1} \rangle \approx 64$ s and $\langle \tau_{\text{run},\infty,1}^2 \rangle \approx 67\ \text{s}^2$ with both quantities rounded to the nearest whole number and taken at the plateau value for the representative experiment corresponding to $D_{\infty,1}$. This provides $D \approx 0.058\ \mu\text{m}^2\ \text{s}^{-1}$, which is similar to experimental values, as indicated in the inset of Fig. 2(c). From now on, we will describe the time evolution of the diffusion coefficient presented in Fig. 2(c) with the two parameters $\langle \tau \rangle$ and $\langle \tau_{\text{run}}^2 \rangle$.

The coefficient of diffusion is not affected by interparticle interactions since experiments are achieved in a dilute regime precluding intercell friction and adhesion. Instead, our results with the WT strain and various mutants depleted or not in EPSs reveal that the amount of released EPSs is key. Moreover, renewal of the population of bacterial cells with the microfluidic setup indicates that the decrease of the diffusion coefficient is due to the modification of the surface properties by previously diffusing cells. In the following we propose a mechanism whereby released EPSs stick on the surface in the form of excreted trails [27,28], which modifies the coefficient of diffusion.

C. Mechanism for the slowdown

The decrease of the coefficient of diffusion and the progressive surface coverage by the trajectories occur on concomitant time scales. Therefore, it is tempting to correlate the surface coverage and the parameters of the model described by Eq. (2). Figure 7 shows that $\langle \tau \rangle$ and $\langle \tau_{\text{run}}^2 \rangle$ vary monotonically with the fraction of distinct sites visited $S(t)$. These two essential temporal parameters, which govern the expression of the diffusion coefficient, may be a function of the probability $P(t)$

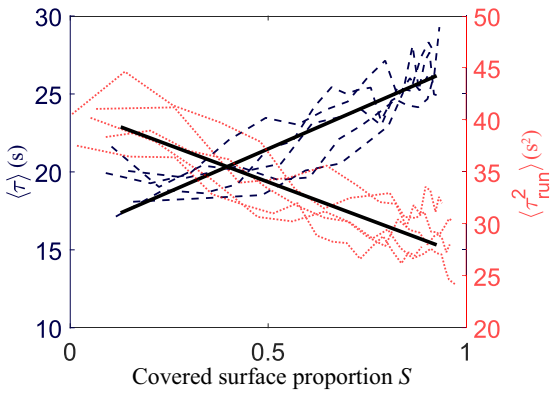

FIG. 7. Variation of $\langle\tau\rangle$ (dashed lines) and $\langle\tau^2_{\rm run}\rangle$ (dotted lines) as functions of the fraction of distinct visited sites $S(t)$ for five different experiments. The solid lines are linear interpolations.

to be located on a surface coated by an extracellular matrix. By approximating $P(t) \approx S(t)$, both parameters can be written simply as a weighted sum of the covered surface such as $\langle\tau\rangle \approx \langle\tau_{glass}\rangle[1 - S(t)] + \langle\tau_{\rm EPS}\rangle S(t)$, with the same formula for $\tau^2_{\rm run}$ instead of each τ.

The computation of $S(t)$ for N random walkers pertains to a class of longstanding problems [29]. Here, both the number of diffusing bacterial cells and the coefficient of diffusion are time dependent and the empirical formula

$$S(t) = 1 - e^{-t/\tau_S} \tag{3}$$

is used to describe experimental data, resulting in a convenient fit with $\tau_S = 1150 \pm 6$ s $< \tau_N$ [Fig. 6(a)]: Most of the surface is visited before sedimentation is complete.

Then, plugging Eq. (3) into the expression for $\langle\tau\rangle$ and $\langle\tau^2_{\rm run}\rangle$ as above yields a numerical estimate of the temporal evolution of $D(t)$ from Eq. (2), which can be compared to measurements. Figure 2(c) indicates good agreement. Therefore, the present analysis implies that the slowdown of the diffusive dynamics can be reasonably attributed to the coverage of the surface by the excreted exopolysaccharides.

Finally, one may ask why cells have longer tumble times and shorter run times on EPSs than on glass. Our results show that the decrease of the diffusion coefficient is not related to viscous drag that could result from the shearing of EPS trails left on the surface, since the average velocity during run periods $\overline{V}_m$ remains constant during the experimental time scale. Moreover, $\overline{V}_m$ is similar for the wild-type strain and for all mutants regardless of their total EPS production rate, confirming that EPSs do not provide additional dissipation during motion. However, it is known that during the early stages of the interaction of the bacterial cells with a surface, cells detect the presence of the extracellular matrix, which induces a positive feedback loop that in turn leads to enhancement of EPS production and cell accumulation [30,31]. For example, *B. subtilis* uses its flagella as mechanosensory organelles for surface sensing. For other microorganisms such as *Myxococcus xanthus*, EPSs play a fundamental role in pilus retraction during social motility [32] and pili-mediated twitching motility is affected by surface stiffness, topography, and chemistry [2,33,34].

Hence, we propose that *Synechocystis* cells sense the EPSs deposited on the surface, which triggers cellular changes that affect the temporal characteristics of run and tumble motion. This is consistent with the description of run and tumble rates from linear response theory for bacteria submitted to spatial changes in concentration of chemicals [35,36].

V. CONCLUSION

The experimental results presented here show a correlation between the diffusive dynamics of the bacterial cells and their propensity for released EPS excretion. The observed slowdown of the diffusion is due to the evolution of the characteristic times of the intermittent dynamics rather than to the enhanced dissipation during the runs due to the viscosity of EPSs. Since the estimated surface fraction of visited sites and the coefficient of diffusion evolve with similar time scales, we propose a model for the decrease of the diffusion coefficient based on the deposition of EPSs on the surface. This suggests strategies for controlling biofilm formation and therefore limiting the infection of host tissues or undesired adhesion in industrial applications.

ACKNOWLEDGMENTS

We thank A. Di Prima and L. Platzer for assistance with the experimental setup and M. Jaharri (LIMSI, Université Paris–Sud) and G. Chau for help with the microfluidic system. We also thank J. Tailleur (MSC, Université Paris–Diderot) for helpful discussions.

APPENDIX A: CALCULATION OF MEAN-SQUARE DISPLACEMENT

In order to study the temporal evolution of the motility, we introduce a time-dependent MSD, which is computed at observation time t for different time intervals Δ as

$$\mathrm{MSD}(t,\Delta) = \frac{1}{N_\delta}\sum_{i=1}^{N_\delta}\frac{1}{2\delta-\Delta}\sum_{t'=t-\delta+\Delta/2}^{t+\delta-\Delta/2}\left[X_i\left(t'+\frac{\Delta}{2}\right) - X_i\left(t'-\frac{\Delta}{2}\right)\right]^2, \tag{A1}$$

where δ is half the time separating two successive values of t and N_δ is the number of active particles between times $t - \delta + \Delta/2$ and $t + \delta - \Delta/2$. The long-time limit of the diffusion is described by computing the ensemble- and time-averaged MSDs, as defined in Eq. (A2), where N is the total number of particles, T_i the trajectory length i, $X_i(t)$ the position of the particle i at time t, and Δ a given time interval:

$$\mathrm{MSD}(\Delta) = \frac{1}{N}\sum_{i=1}^{N}\frac{1}{T_i-\Delta}\sum_{t=1}^{T_i-\Delta}[X_i(t+\Delta) - X_i(t)]^2. \tag{A2}$$

APPENDIX B: RUN AND TUMBLE TIMES

Run times $\tau_{\rm run}$ are measured by computing a coarse-grained velocity V_δ at each time point, with δ an adjustable time

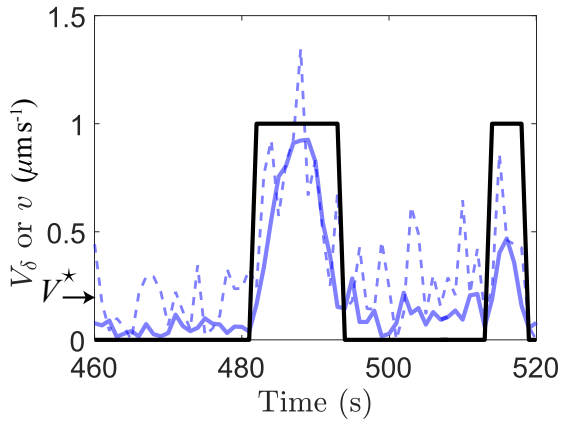

FIG. 8. Coarse-grained velocity V_δ [solid (gray) line] and instantaneous velocity v (dashed line). The black solid line indicates the selection of run periods according to the criteria explained in the text (set to 1 when a run is detected and 0 otherwise). The velocity threshold $V^\star$ is indicated with an arrow.

interval,

$$V_\delta(t) = \frac{|X(t+\delta/2) - X(t-\delta/2)|}{\delta}.$$

An example of such a computation with $\delta = 4$ is shown Fig. 8, where the highest velocity peaks correspond to runs and are separated by tumbles. Run periods are selected according to two different criteria: the velocity $V_\delta > V^\star$ and the distance traveled $\Delta x > \Delta x^\star$, where $V^\star$ and $\Delta x^\star$ are some threshold velocity and length, respectively. Once run periods are accepted, the rest of the trajectory is filled with tumble periods.

The criteria $V^\star = 0.2\ \mu\text{m s}^{-1}$ and $\Delta x^\star = 0.9\ \mu$m [as suggested by tails of the PDF in Fig. 4(b)] provide a faithful distinction between the various types of motion. While the choice of $V^\star$ and $\Delta x^\star$ is somewhat arbitrary, the conclusions based on the use of run and tumble times do not depend significantly on these criteria.

APPENDIX C: NUMERICAL SIMULATIONS

Numerical simulations are based on the Monte Carlo method. Here 453 particles are launched, with trajectories of 969 s. The duration of tumbles and runs is taken from the experimental distributions [Figs. 9(a) and 9(b)], fitted by a

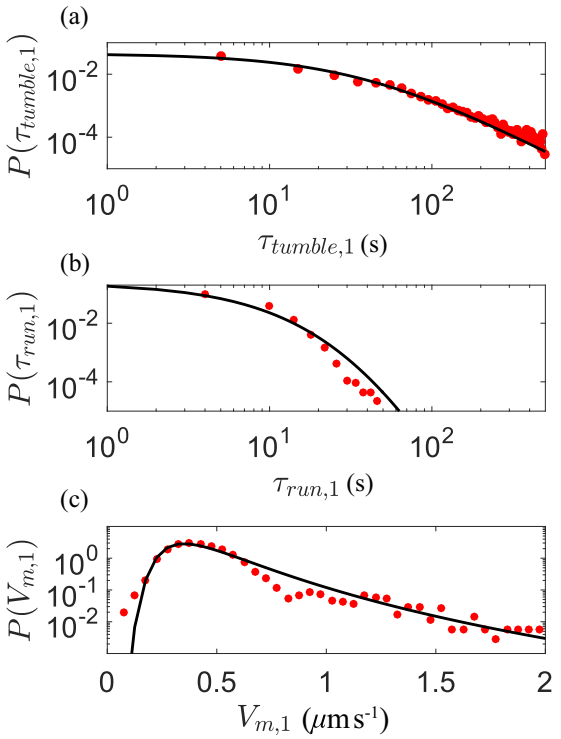

FIG. 9. Distribution of (a) tumble times, (b) run times, and (c) average velocity during runs $V_m = l_{\text{run}}/\tau_{\text{run}}$. Experimental data (points), corresponding to the experiment leading to $D_{\infty,1}$ described in Sec. III B, are fitted with expressions given in Appendix C (solid lines), which are used for numerical simulations.

power law of the form

$$P(\tau_i) = \frac{\alpha_i}{A_i} \frac{1}{\left(1 + \frac{\tau_i}{A_i}\right)^{1+\alpha_i}},$$

with $A_{\text{tumble}} = 38$ s, $\alpha_{\text{tumble}} = 1.7$, $A_{\text{run}} = 42$ s, and $\alpha_{\text{run}} = 11$. The tumble motion is simulated by making a given particle jiggle in the polar system of coordinates whose center is the fixed position between two runs. The coordinates (r,θ) are chosen such that θ is random and r is selected in an exponential distribution of mean $\lambda_{\text{tumble}} = 0.19\ \mu$m. The run motion is defined by ballistic excursions of duration τ_{run}, during which the traveled distance is $l_{\text{run}} = V_m \tau_{\text{run}}$, where τ_{run} is selected from $P(\tau_{\text{run}})$ and V_m is chosen from a generalized extreme value probability law, which conveniently fit the experimental distribution [Fig. 9(c)]. This law is defined with a location parameter $\mu = 0.37\ \mu\text{m s}^{-1}$, a scale parameter $\sigma = 0.13\ \mu\text{m s}^{-1}$, and a shape parameter $k = 0.17$. The angle between two successive runs is random.

[1] S. Singh, S. K. Singh, I. Chowdhury, and R. Singh, Open Microbiol. J. **11**, 53 (2017).
[2] H. H. Tuson and D. B. Weibel, Soft Matter **9**, 4368 (2013).
[3] D. Davies, Nat. Rev. Drug Discov. **2**, 114 (2003),
[4] J. W. Costerton, Science **284**, 1318 (1999).
[5] A. Omar, J. Wright, G. Schultz, R. Burrell, and P. Nadworny, Microorganisms **5**, 9 (2017).
[6] M. G. Mazza, J. Phys. D **49**, 203001 (2016).
[7] J. Taktikos, Y. T. Lin, H. Stark, N. Biais, and V. Zaburdaev, PLoS One **10**, e0137661 (2015).
[8] H. Vlamakis, Y. Chai, P. Beauregard, R. Losick, and R. Kolter, Nat. Rev. Microbiol. **11**, 157 (2013).
[9] K. C. Marshall, R. Stout, and R. Mitchell, Microbiology **68**, 337 (1971).

[10] T. Jittawuttipoka, M. Planchon, O. Spalla, K. Benzerara, F. Guyot, C. Cassier-Chauvat, and F. Chauvat, PLoS One **8**, e55564 (2013).
[11] T. Ursell, R. M. W. Chau, S. Wisen, D. Bhaya, and K. C. Huang, PLoS Comput. Biol. **9**, e1003205 (2013).
[12] K. Zhao, B. S. Tseng, B. Beckerman, F. Jin, M. L. Gibiansky, J. J. Harrison, E. Luijten, M. R. Parsek, and G. C. L. Wong, Nature (London) **497**, 388 (2013).
[13] A. Gelimson, K. Zhao, C. K. Lee, W. T. Kranz, G. C. L. Wong, and R. Golestanian, Phys. Rev. Lett. **117**, 178102 (2016).
[14] W. Hu, M. L. Gibiansky, J. Wang, C. Wang, R. Lux, Y. Li, G. C. L. Wong, and W. Shi, Sci. Rep. **6**, 17790 (2016).
[15] J. M. Panoff, B. Priem, H. Morvan, and F. Joset, Arch. Microbiol. **150**, 558 (1988).
[16] D. Bhaya, N. R. Bianco, D. Bryant, and A. Grossman, Mol. Microbiol. **37**, 941 (2000).
[17] W.-O. Ng, A. R. Grossman, and D. Bhaya, J. Bacteriol. **185**, 1599 (2003).
[18] R. M. W. Chau, T. Ursell, S. Wang, K. C. Huang, and D. Bhaya, Biophys. J. **108**, 1623 (2015).
[19] A. Wilde and C. W. Mullineaux, Mol. Microbiol. **98**, 998 (2015).
[20] H. C. Berg, N. Darnton, and J. Jaffe, http://www.rowland.harvard.edu/labs/bacteria/software/index.php.
[21] D. Glaser and M. Higgins, J. Bacteriol. **171**, 669 (1989).
[22] H. C. Berg and D. A. Brown, Nature (London) **239**, 500 (1972).
[23] O. Bénichou, C. Loverdo, M. Moreau, and R. Voituriez, Rev. Mod. Phys. **83**, 81 (2011).
[24] A. Touhami, M. H. Jericho, J. M. Boyd, and T. J. Beveridge, J. Bacteriol. **188**, 370 (2006).
[25] E. Montroll and G. Weiss, J. Math. Phys. **6**, 167 (1965).
[26] J. P. Bouchaud and A. Georges, Phys. Rep. **195**, 127 (1990).
[27] A. Ducret, M.-P. Valignat, F. Mouhamar, T. Mignot, and O. Theodoly, Proc. Natl. Acad. Sci. U.S.A. **109**, 10036 (2012).
[28] R. Yu and D. Kaiser, Mol. Microbiol. **63**, 454 (2007).
[29] H. Larralde, P. Trunfio, H. E. Stanley, and G.H. Weiss, Nature (London) **355**, 423 (1992).
[30] F. Rossi and R. De Philippis, Life **5**, 1218 (2015).
[31] N. Steinberg and I. Kolodkin-Gal, J. Bacteriol. **197**, 2092 (2015).
[32] Y. Li, H. Sun, X. Ma, A. Lu, R. Lux, D. Zusman, and W. Shi, Proc. Natl. Acad. Sci. U.S.A. **100**, 5443 (2003).
[33] B. Maier and G. C. L. Wong, Trends Microbiol. **23**, 775 (2015).
[34] V. Zaburdaev, N. Biais, M. Schmiedeberg, J. Eriksson, A. B. Jonsson, M. P. Sheetz, and D. A. Weitz, Biophys. J. **107**, 1523 (2014).
[35] P.-G. de Gennes, Eur. Biophys. J. **33**, 691 (2004).
[36] J. E. Segall, S. M. Block, and H. C. Berg, Proc. Natl. Acad. Sci. USA **83**, 8987 (1986).